Research Article | Vol. 10, No. 12 / 1 December 2019 / Biomedical Optics Express 6462
Biomedical Optics EXPRESS

Sample drift estimation method based on speckle patterns formed by backscattered laser light

SHIH-YA CHEN,[1] RAINER HEINTZMANN,[2,3] AND CHRISTOPH CREMER[1,4,*]

[1] *Institute of Molecular Biology, Mainz, Germany*
[2] *Institute of Physical Chemistry and Abbe Center of Photonics, Friedrich-Schiller-University Jena, Jena, Germany*
[3] *Leibniz Institute of Photonic Technology, Jena, Germany*
[4] *Department of Physics, University of Mainz (JGU), Mainz, Germany*
[*] *cremer@kip.uni-heidelberg.de*

Abstract: Single molecule localization microscopy (SMLM) has been established to acquire images with unprecedented resolution down to several nanometers. A typical time scale for image acquisition is several minutes to hours. Yet it is difficult to avoid completely sample drift for long time measurements. To estimate drift, we present a method based on the evaluation of speckle patterns formed by backscattered laser light from the cells using a single molecule localization microscope setup. A z-stack of unique speckle patterns is recorded prior to the measurements as a three-dimensional position reference. During the experiment, images of scattered laser light were acquired, and correlated individually with each of the images of the speckle reference stack to estimate x, y and z drift. Our method shows highly comparable results with a fiducial marker approach, achieving a precision of several nanometers. This method allows for high precision three dimensional drift correction of microscope systems without any additional sample preparation.

1. Introduction

Single molecule localization microscopy (SMLM) was developed to achieve super-resolved microscopy images with unprecedented resolution down to several nanometers [1–4]. However, sample drift occurs commonly during image acquisition. A small amount of drift in the microscope system can induce blurring artifacts in the reconstructed image, hampering resolution. This is especially disadvantageous in 3D SMLM where the reconstructed 3D image depends critically on the correct axial coordinate. Therefore, correction of sample drift is essential and several approaches were presented to correct sample drift in microscope systems.

One of the most common approaches is based on image post-processing using cross-correlation of the fluorescence emission localization data[5–7]. This method sorts blinking molecules in time intervals of an equal length. The combined blinks in each time interval form a 3D structure. The cross-correlation of the 3D structures of every time interval with the corresponding reference structure of the first time interval will yield the drift during the experiment. The position of the detected molecules is then adjusted according to the result of the computed drift. However, this method requires a sufficient number of blinking events in the reconstructed images to provide visible features for the calculation. Biological targets with distinct features such as filaments, a fiber-like structure, may result in better drift accuracy compared to samples without clear structures.

Another common approach is to prepare fiducial markers on the coverslips such as gold nanoparticles or fluorescent beads [8,9]. By tracking the positions of the fiducial markers, the

#374592 https://doi.org/10.1364/BOE.10.006462
Journal © 2019 Received 2 Aug 2019; revised 28 Oct 2019; accepted 4 Nov 2019; published 25 Nov 2019

Biomedical Optics EXPRESS

drift of the microscope system in three dimensions is obtained. The advantage of this drift correction method is that biological features in the images are not required. However, fiducial markers need to be prepared before the preparation of the samples. Additional optimization of sample preparation for the fiducial markers is recommended to prevent aggregation and inhomogeneous distribution of the markers on the coverslip, which has undesired influence on finding appropriate markers for drift correction [10].

An alternative approach for drift correction is to fabricate a fiduciary micro-pattern by the means of a lithography method [11]. Manufacturing directly imprinted coverslips significantly reduces the effort of sample preparation, but they might not be easily accessible and affordable for standard bio-imaging laboratories.

A hardware-based approach is to introduce an infrared LED light source in the microscope system. By detecting the reflection at the interface between the cover glass and the embedding medium, the axial position is tracked and constantly adjusted during image acquisition [12]. This method presents a convenient axial drift correction and focus stabilization for microscope users. However, an additional lateral drift correction method should be applied in order to realize a three dimensional correction.

An alternative approach is based on image correlation using bright-field images of samples illuminated by an infrared LED. This approach provides an advanced method to simultaneously correct drift in three dimensions [13]. This method requires an additional light source for illumination and sufficient features in the bright-field images for a correlation analysis.

In this report, we present a method for SMLM based on speckle pattern image correlation to estimate sample drift in three dimensions. A home-built microscope setup equipped with laser light sources was used to demonstrate the drift estimation method. Using only low power of the laser, the interference of the backscattered laser light of a cell sample results in a speckle pattern in the acquired image. Due to the complexity of cells, the speckle pattern is unique and varies strongly with focus position. Therefore, the speckles can be used to provide a straightforward positioning reference for the drift estimation measurements. By recording a z-stack of images showing laser speckles, the three dimensional position information of the cell sample is encoded in this reference stack. We used an image registration method based on nonlinear optimization and discrete Fourier transforms (DFTs) [14]. This method can achieve high accuracy without demanding computational time and memory. By correlating the scattered laser images individually with each of the images from the speckle reference stack using the DFT method will yield x, y and z drift information. Below we describe our method to determine accurately the 3D sample position and validate it on fiducial markers (fluorescent beads) experiments. Additionally, a 3D SMLM image of a cell sample is presented to demonstrate our drift correction approach.

2. Methods

2.1. Experimental setup

A home-built SMLM based on the setup presented in [15] was used to acquire images for the proposed drift estimation method. The scheme of the setup is shown in Fig. 1. The microscope was equipped with a 488 nm (Omicron, Germany), a 561 nm (Frankfurt Laser, Germany) and a 647 nm (Cobolt, Sweden) laser. A telescope consisting of two lenses L1 (f = 30 mm, Thorlabs) and L2 (f = 60 mm, Thorlabs) was used to expand the laser beam. A quad band dichroic (Chroma, zt405/488/561/647rpc) was used to reflect the lasers. A tube lens (f = 120 mm, Thorlabs) was utilized to focus the beam into the back focal plane of the objective lens (HCX PL APO 100×/NA 1.47 OIL, Leica) mounted in a nanometer positioning piezo stage (P-721, Physik Instrumente). The immersion oil with a refractive index of 1.518 (at 23°C, Zeiss) was applied on the objective lens. The samples were placed on a manually controlled x-y stage. The focus was adjusted

Biomedical Optics EXPRESS

using a manual z-axis translation mount (SM1Z, Thorlabs) and the white light LED was used for bright-field illumination.

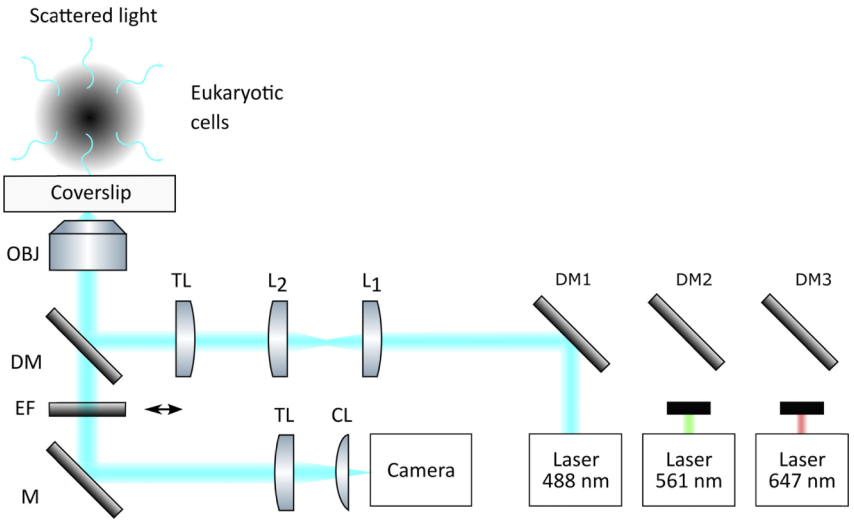

Fig. 1. Demonstration of imaging speckle patterns using a standard SMLM setup. (Obj: objective lens, DM: dichroic mirror, EF: emission filter for fluorescent beads measurement and for 3D SMLM, M: mirror, TL: tube lens, CL: cylindrical lens, L: lens)

A tube lens (f = 200 mm, Thorlabs) was used to image the sample onto a sCMOS camera (PCO edge 4.2, PCO). A cylindrical lens (f = 1000 mm, Thorlabs) was used in the detection beam path to introduce astigmatism for 3D localization. Three emission filters (HC520/35 Semrock, ET600/50 Chroma, ET655 Chroma) were mounted in a PC controlled motorized filter wheel (FW102C, Thorlabs). An emission filter was inserted for fluorescent beads measurements and SMLM measurements. No emission filter was used for the speckle mode.

2.2. Speckle patterns of a cell

Speckle patterns originate from the interference of coherent light showing intensity variations in pronounced features [16]. Such a phenomenon can also be observed when illuminating biological samples [17]. To obtain a speckle pattern of a cell, the optical setup shown in Fig. 1 was used to illuminate a eukaryotic cell.

To acquire a speckle pattern, the emission filter was removed and the backscattered light from the sample was recorded on the camera. An exemplary speckle image is shown in Fig. 2. A complex intensity distribution, formed by the interference of the backscattered laser, can be realized. These speckle patterns are unique, because each of the cells exhibits a huge variety of structural formations. When the sample drifts, the speckle pattern is shifted accordingly and the amount of drift can be estimated with high accuracy using an image registration method [13]. Bright signals, originating from reflected light from the optical elements, can increase the background of the image and reduce the speckle contrast. In most cases, the speckle contrast is sufficiently high to determine reliably the sample drift by image registration.

The speckle size is defined as [18]:

$$d = 2.44\ \lambda\ f_{\#} M \tag{1}$$

where the λ is the wavelength, $f_{\#}$ is the f-number of the lens system and M is the magnification. This relation implicates, that a laser with a longer wavelength produces a speckle pattern with a larger speckle size, which can lower the precision of the image registration.

Biomedical Optics EXPRESS

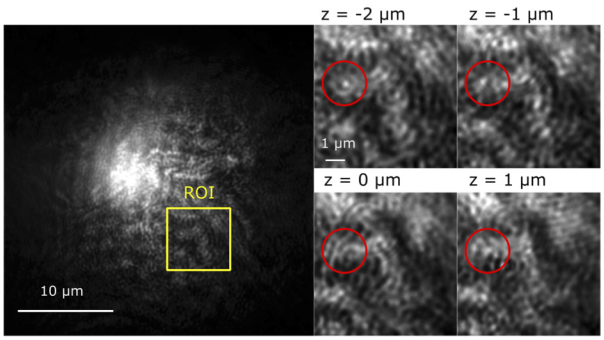

Fig. 2. Speckle pattern of a cell sample. The insets show the ROI at four axial positions (z = - 2 µm, −1 µm, 0 µm and 1 µm). A speckle feature is highlighted by a red circle.

The insets of Fig. 2 show the speckle pattern of the cell sample at four z-positions with a relative axial separation of 1 µm. A nearly diffraction limited spot indicated with a red circle can be seen at the position of z = −2 µm. At the position of z = −1 µm the spot is not visible anymore instead a new spot at a slightly shifted position appeared.

2.3. Drift estimation algorithm

Since each cell exhibits a unique speckle pattern and the speckle patterns vary continuously in z, the speckle patterns can be used as a position reference of the sample in three dimensions. Prior to the drift measurement, a position reference stack containing speckles at different axial planes is recorded. As shown in Fig. 3, a speckle reference z-stack f with n frames and a separation of Δz was acquired at time t_0, where z represents the axial position of each speckle frame.

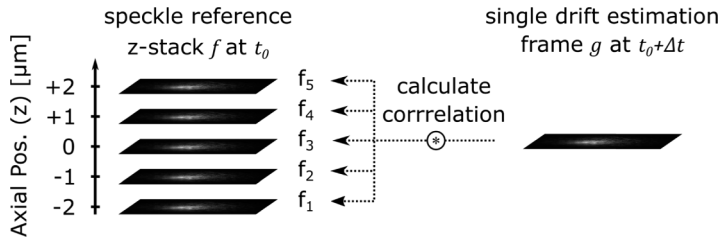

Fig. 3. Scheme for drift estimation. A z-stack of speckle patterns f as a position reference of the cell is acquired. Single drift estimation frames g are captured at regular time intervals during the experiment. By finding the maximum correlation in the speckle reference stack f with g, the drift in x, y and z is estimated.

For drift estimation, single drift estimation frames g were acquired separated in time by Δt. The time separation depends on the SMLM experiment. Each of these images g show a speckle pattern closely corresponding to one present in the speckle reference stack f. Axial and lateral drift is determined by computing the lateral (xy-) maximum of the correlation between g and each frame $f(z)$. The z-position of the speckle reference frame with the highest correlation corresponds to the axial position of the measured drift estimation frame g.

For evaluating the correlation R between g and $f(z)$, we used the DFT method according to [13]. The DFT algorithm returns the image displacement vector $D = [x + \Delta x, y + \Delta y]$ by correlating the single drift estimation frame g with every frame of f:

$$CC_{xy} = \mathrm{DFT}_{xy}^{-1}(\mathrm{DFT}_{xy}(f(z))\mathrm{DFT}_{xy}^{*}(g)), \tag{2}$$

Biomedical Optics EXPRESS

$$D(z) = \text{argmax}_{xy} \, |CC_{xy}|. \tag{3}$$

Additionally the DFT algorithm returns the translation invariant normalized root mean square error (RMSE) DFT_{ERROR} between the two images:

$$DFT_{ERROR} = \sqrt{1 - \frac{max_{xy}|CC_{xy}|^2}{\sum |DFT_{xy}(f(z))|^2 \sum |DFT_{xy}(g)|^2}}. \tag{4}$$

The normalized correlation value is calculated as

$$R_{DFT}(\text{z}) = 1 - DFT_{ERROR}(f(\text{z}), g). \tag{5}$$

For higher accuracy, an upsampling factor of 100 was used for the DFT and R_{DFT} was interpolated four times along z using cubic spline interpolation. In the following experiments, all data analysis was performed using Matlab R2018b (Mathworks). Since the position of a cell is defined by recording a reference z-stack, a fine step size of the reference stack can encode the detailed speckle patterns. A step size of 10 nm was used to acquire the z-position in the following measurements. The z-position can be estimated precisely by computing the normalized correlation value as shown in Eq. 5.

2.4. Sample preparation

To calibrate the single molecule axial localization based on astigmatism, a sample with fluorescent beads (TetraSpeck 100 nm, ThermoFisher) was prepared. Fluorescent beads were diluted 1:1000 in ddH_2O. The suspension beads solution was sonicated in an ultrasonic bath (EMAG) for 15 min to prevent aggregation. 200 µl beads solution was applied on a glass bottom 35 mm dish (ibidi) overnight. The dish was washed with ddH_2O water extensively about 10 times to remove mobile beads. After applying 1 ml ddH_2O in the dish, the fluorescent beads sample was used for 3D calibration based on the method [19, 20].

To validate our method, we compared the SMLM localizations with our speckle-based drift estimation on cell samples including fluorescent beads. A sample with fluorescent beads located on the coverslip prior to seeding the cells was prepared as described above. U2OS cells were cultured in a 25 ml culture flask filled with Dulbecco's Modified Eagle's Medium (DMEM, Thermo Fisher) supplemented with 10% fetal bovine serum (FBS, Thermo Fisher) and 1% Penicillin Streptomycin (Pen Strep, Thermo Fisher) in a cell culture incubator (37°C, 5% CO_2). Cells were plated at low confluency on the dish prepared with immobilized beads overnight. Cells were fixed with pre-warmed (37°C) Formaldehyde (4%, Sigma-Aldrich) for 15 min. Afterwards cells were washed three times with Dubecco's Phosphate Buffered Saline (DPBS, Sigma-Aldrich) and the cells were embedded in PBS for imaging.

To image the cell nucleus, the U2OS cells were treated with 0.5% Triton X-100 in DPBS for 10 min and washed with DPBS. Cells were incubated at 37 °C with 1:1000 RNase A cocktail (Thermo Fisher) in DPBS for 15 min. Cells were washed with DPBS and nuclei were stained with 0.05 µM SytoxOrange in PBS (Thermo Fisher) for 30 min. A typical imaging buffer with an enzymatic oxygen scavenging system was prepared for fBALM [21]. The buffer contained 10% glucose (Sigma-Aldrich), 5 mg/ml glucose oxidase from aspergillus niger (Sigma-Aldrich), 500 µg/ml catalase from bovine liver (Sigma-Aldrich) in DPBS.

2.5. Determination of 3D positions of fluorescent beads

To determine the 3D position information of fluorescent beads from a 2D image, a cylindrical lens was inserted in the detection beam path of the optical setup to deform the point spread function (PSF) to an elliptical shape with increasing defocus [19,20]. To derive the axial position of the fluorescent beads, a calibration of the setup is necessary. For this calibration, a z-stack

Biomedical Optics EXPRESS

with an axial range from −400 nm to 400 nm and a step size of 10 nm of the 3D PSFs of three fluorescent beads in the center of the field of view was recorded. This image stack was processed using ThunderSTORM to acquire the 3D calibration curve [22]. The calibration curve was used to determine the 3D position of fluorescent beads from 2D images using ThunderSTORM.

2.6. Drift estimation routine for SMLM imaging

To demonstrate the drift correction method based on speckle patterns for SMLM measurements, an experimental flow chart is presented in Fig. 4. Before the SMLM measurement, the focal position of the cell Pos_{center} and the beads Pos_{beads} were identified. For the speckle-based method, no emission filter was inserted and a reference z-stack at Pos_{center} was acquired.

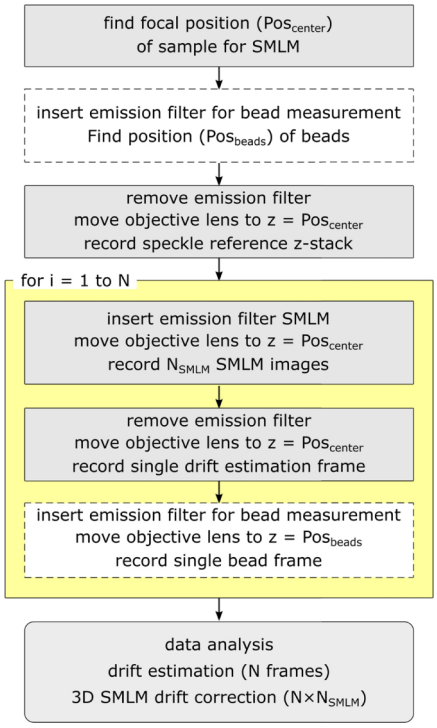

Fig. 4. Flow chart of 3D SMLM experiment with speckle- and beads-based drift estimation methods. The dashed boxes are optional and are only used for comparison measurements.

In the next step, we acquired N_{SMLM} images at position Pos_{center} with an emission filter inserted into the detection beam path. Afterwards, a single drift frame was acquired at position Pos_{center} without an emission filter. Then a single bead frame was acquired at position Pos_{beads} with an emission filter. This measurement procedure of the last three steps is an N times routine and can be defined according to requirements of the user. The amount of drift determined by both methods were analyzed according to Section 2.3 and Section 2.5. The results of the drift estimation method based on the speckle method were interpolated to the number of total frames $N \times N_{SMLM}$ of the SMLM measurement using spline interpolation. The positions of the localized molecules were then corrected according to the drift.

Alternatively, the experiment can be performed using a single laser. For speckle illumination, the emission filter is removed and the laser power is reduced to prevent overexposure of the camera. For SMLM, the emission filter is inserted and the laser illumination intensity is increased to achieve appropriate blinking of molecules. The operation duration to insert a filter takes

Biomedical Optics EXPRESS

about 3 to 4 seconds using the default setting of the filter wheel. A shorter operation time can be achieved using the fast mode, or reducing the pause time or customization of in sthe routine setting of the filter wheel, or using a second camera and ND-filters or weak reflections for speckle-based drift estimation. Because the intensity of the speckle pattern is much higher than the intensity of the fluorescent emission of the excited fluorophores, the blinking emission does not influence the accuracy of the image registration.

3. Drift estimation experiments

Two different experiments were performed to show the performance of the drift estimation algorithm. One experiment was done on a short time scale to show the typical characteristics of the proposed correlation method. The other experiment was performed on a long time scale to compare the results of our methods with the drift estimation method using fluorescent beads.

3.1. Simulated drift using a cell sample

The sample (U2OS cells) was illuminated using the 488 nm laser with a power of 0.01 mW (1.4 W/cm^2) in the speckle mode. A speckle reference z-stack f_{exp1} with a range of 10 µm and a step size of 10 nm was acquired with a camera exposure of 5 ms. To demonstrate the correlation of speckle patterns, a second stack g_{exp1} of speckle images representing simulated drift estimation frames at 27 axial positions starting at - 2.75 µm with a step size of 250 nm was recorded immediately after the first stack with the same exposure time and laser power.

3.2. Cell sample with fluorescent beads

To validate our method, the sample (U2OS cells with fluorescent beads) was imaged sequentially between the method based on speckle patterns and the fluorescent beads method. At each of the measurements, we acquired an image showing a speckle pattern and sequentially another image showing beads by immediately inserting the emission filter using the filter wheel. The switching time between the image acquisitions was about 2 seconds. We analyzed the positions between the two methods.

To acquire speckle patterns, the power of the laser with a wavelength of 488 nm was set to 0.01 mW (1.4 W/cm^2) and 10 ms exposure to record a reference stack spanning 500 nm at a step size of 10 nm. The 488 nm laser corresponding to an irradiance (8 mW∼1 kW/cm^2) was used to acquire fluorescence of the beads with a camera exposure of 100 ms.

The drift estimation based on speckle patterns was analyzed according to Section 2.3. The 3D positions of three fluorescent beads were determined using ThunderSTORM. The analysis is shown in a time trace and a comparison of the results is presented in Section 4.3.

3.3. Drift correction for SMLM of nuclear structure

For the demonstration of the speckle-based method used for imaging chromatin structures, the speckle images were acquired using the same setting described in Section 3.2. For imaging beads as a comparison experiment, the laser with a wavelength of 647 nm (8 mW, ∼1 kW/cm^2) and a camera exposure of 30 ms were used. The emission filter LP655 was selected. Four fluorescent beads were analyzed using ThunderSTORM.

For SMLM imaging, the drift estimation routine described in Section 2.6 was utilized. Prior to the acquisition routine, a reference z-stack with an axial range of 410 nm and a step size of 10 nm was acquired using the laser with a wavelength of 488 nm. For the super-resolution imaging of the chromatin structure, the laser with a wavelength of 561 nm (14 mW, ∼1 kW/cm^2) was used to induce blinking events. Twenty subsets of 500 images were acquired and the localized molecules were analyzed using ThunderSTORM.

Biomedical Optics EXPRESS

4. Results

4.1. Experimental result of the simulated drift using a cell sample

To validate our drift estimation method, we performed an experiment with the U2OS cells sample without fluorescent beads. Figure 5 shows a typical curve of the correlation between $g_{exp1}(z = 0)$ and each frame of f_{exp1} yielding a clear maximum, which represents an estimation of the z position of the sample. Since Fig. 5 was based on data acquired immediately after recording the reference stack, almost no drift was present and therefore the maximum is as expected close to the position $z = 0$.

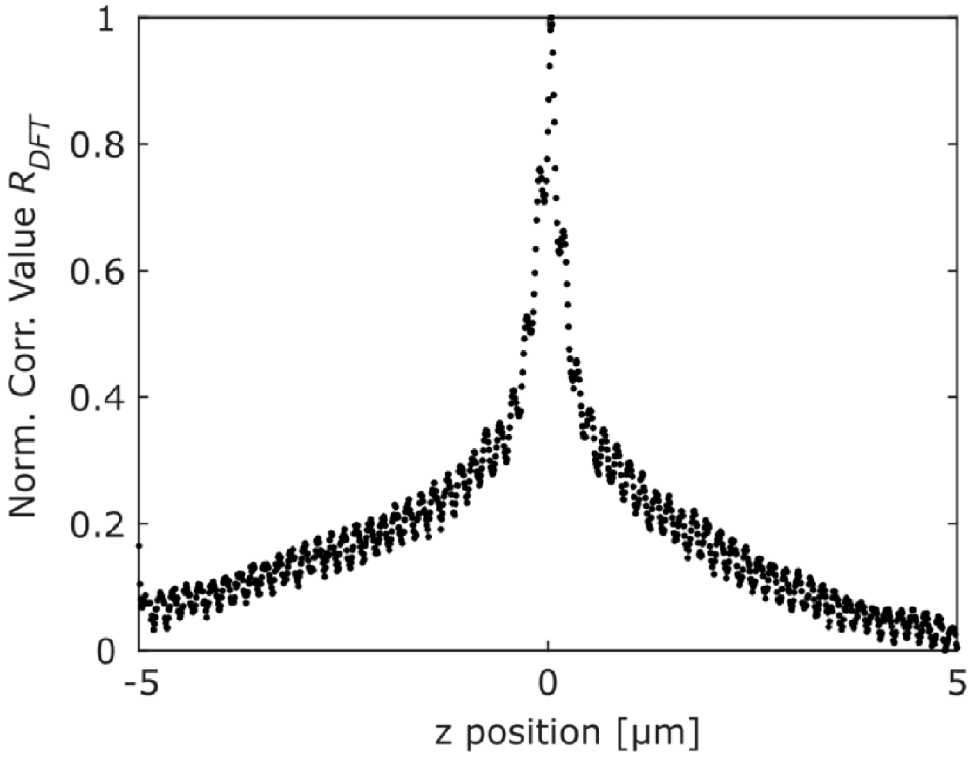

Fig. 5. Correlation (normalized to a maximum of one) between the drift estimation frame $g_{exp1}(z = 0)$ and each image of the speckle reference z-stack f obtained from measured data.

To evaluate our speckle-based method for larger drifts, all frames of g_{exp1} were correlated with f_{exp1} and the z position of the maximum correlation was determined. Since the axial position of every frame of g_{exp1} is known and the drift of the setup can be neglected, a linear dependency can be found between the axial positions versus the position determined by our drift estimation algorithm as shown in Fig. 6(a). The residuals after linear regression are shown in Fig. 6(b) yielding a standard deviation of 2 nm, indicating that the proposed drift correction method can robustly correct simulated drift with high accuracy.

4.2. Repeatability of the drift estimation

The repeatability of the drift estimation was investigated by acquiring speckle patterns continuously for 10 seconds at the same position, assuming no drift happened during this image acquisition. A stack of 1000 images (10 ms per frame) was captured and the stack of speckle patterns was then analyzed using the method described in Section 2.3. As shown in Fig. 7, the standard deviation

Biomedical Optics EXPRESS

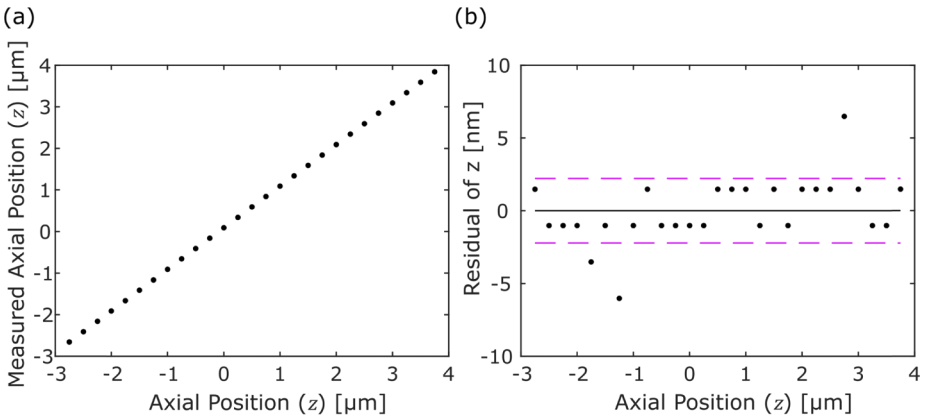

Fig. 6. Speckle based z-position estimation by a defined z-position with a range of 7 µm and a 250 nm step size. (a) Measured z-position. (b) Residuals of the linear regression.

of the repeatability of the speckle-based drift estimation in axial position are 3.0 nm and 1.5 nm in the x-axis and 2.2 nm in the y-axis. In Fig. 7(a), a peak at one second with a z-drift of 16 nm can be seen. This may be attributed to environmental conditions such as airflow or a small vibration of the optical table.

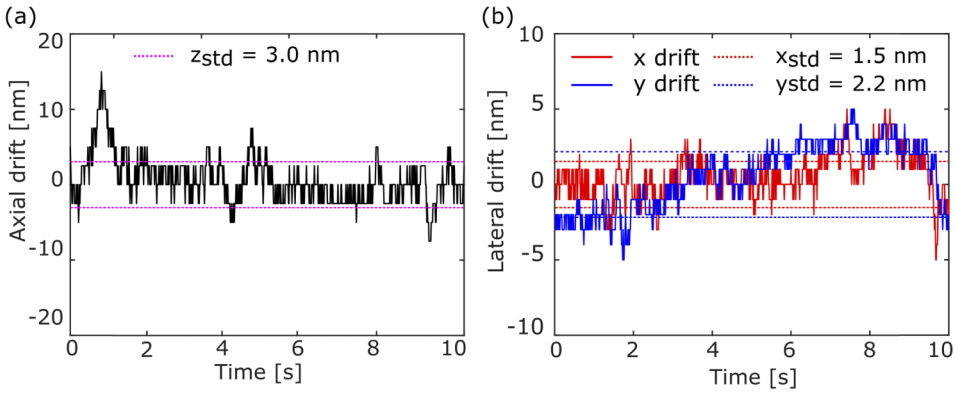

Fig. 7. The repeatability of the speckle-based drift estimation method for 10 seconds in (a) optical axis (z) and (b) lateral axes (x,y).

4.3. Experimental results of the cell sample with fluorescent beads

To validate our method for a practical drift situation, we compared the speckle-based method and the localized positions of fluorescent beads. The images of fluorescent beads can be considered as single emitters shown in the raw images of SMLM measurements. The experiment was performed as shown in the flow chart in Fig. 4 without the SMLM image acquisition. We acquired pairs of images showing speckles and fluorescent beads every 20 seconds in a period of 10 minutes. An exemplary speckle image is shown in Fig. 8(a). Three fluorescent beads as indicated in the ROI of Fig. 8(b) were used for the analysis.

The comparison of the two drift estimation methods is shown in Fig. 9. Figure 9(a) shows the axial drift determined by evaluating the fluorescent beads and by using our drift estimation method. A steady drift of 100 nm could be seen in the first 5 minutes. After 5 minutes, the system does not exhibit a noticeable drift. The shaded range of 5.4 nm is given by the averaged

Biomedical Optics EXPRESS

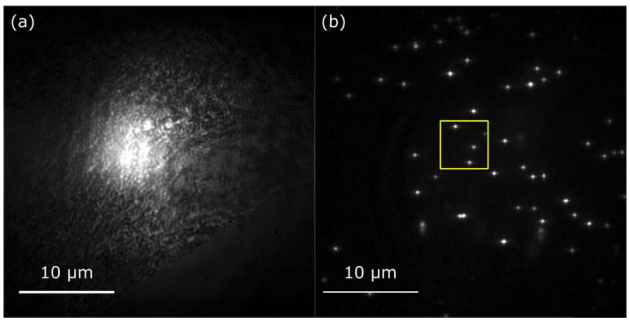

Fig. 8. An experimental result of the sample drift measurement. A pair of image with (a) a speckle pattern and (b) fluorescent beads.

standard deviation of all bead localizations and the results of both methods correspond closely. We defined the localization-based fluorescent bead method as the references and compared it with the results based on the speckle image correlation. The axial position difference between both methods is shown in Fig. 9(b) with a standard deviation of ± 9.4 nm. Although this value is good enough for SMLM experiments, it also indicates that the estimate of 2 nm precision as obtained from Fig. 6 may be overly optimistic.

A similar analysis was applied to determine the lateral drift in x and y and the results are shown in Fig. 9(c). The measurement shows that the microscope system has a gradual drift of about 150 nm in 10 minutes in the x direction. A small drift of the system in the order of tens of nanometers can be seen in the y direction. The shaded area indicates the average standard deviation of the bead measurement of ± 1.7 nm and ± 3.7 nm in x and y, respectively. The results of the differences between the two methods in x and y are shown in Fig. 9(d) with a standard deviation of ± 6.4 nm and ± 8.2 nm in x and y, respectively.

The results of the lateral and axial drift using speckle image correlation show a good agreement with the results using fluorescent beads. The small deviation between the two methods can be explained by small disturbances introduced by the rotation of the filter wheel. The repeatability of the drift estimation as shown in Fig. 7 caused by environmental conditions could lead to also this small deviation. Both methods have several nanometer precision but our speckle pattern image registration method does not require additional sample preparation and is highly applicable for SMLM measurements.

4.4. Drift correction for 3D SMLM

Nuclei labeled with the DNA dye SytoxOrange were used to demonstrate the speckle-based drift correction. Fluorescent beads were prepared additionally in the dish for a comparison measurement. The results of the drift estimation comparison between the two methods is shown in Fig. 10. The drift estimations in three dimensions show a good agreement between the two methods. A lower precision of the fluorescent beads compared with the results shown in the Fig. 9 can be attributed to a lower intensity of the fluorescent beads in the sample.

Figure 11 reveals nuclear genome architecture with small nucleosome domain clusters. Similar patterns were realized in [21,23]. As shown in the inset of Fig. 11, before correction, the nucleosome domain cluster shown in the center appears to be distributed spatially in a broad range along the axial direction. Whereas, after drift correction, a much smaller distribution of the nucleosome cluster can be observed as indicated by the reduced color distribution. The proposed drift correction method may support biological studies of nuclear genome architecture for a better quantification of the chromatin nano-organization inside the nucleus.

Biomedical Optics EXPRESS

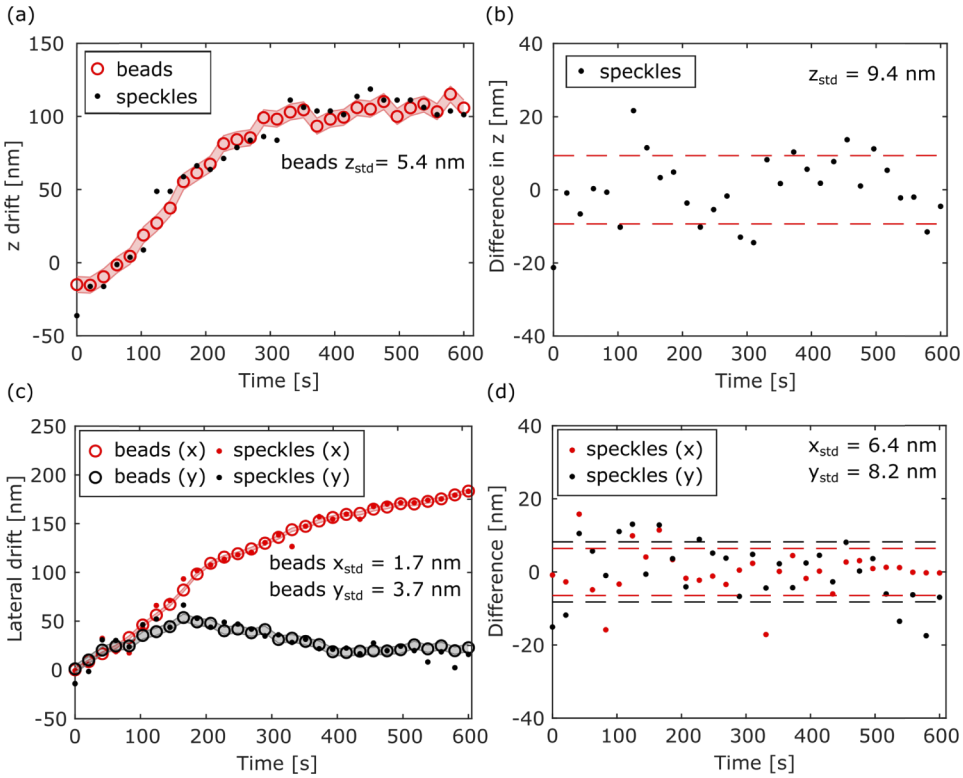

Fig. 9. Time dependent measurement for comparing the drift estimation between fluorescent beads and our speckle-based method. The sample was illuminated by the laser with a wavelength of 488 nm. (a,c) Axial and lateral drift measurements. The shaded areas are given by the averaged standard deviation of all bead localizations. (b,d) Difference between beads- and speckle-based drift estimation in axial and in lateral direction. The dashed lines indicate the standard deviation.

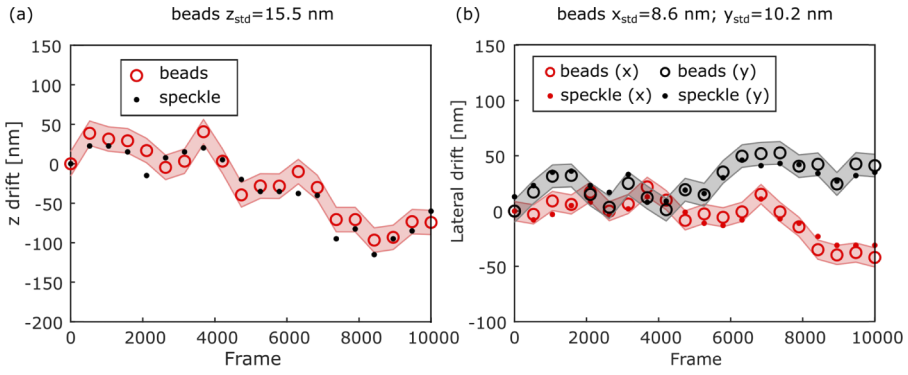

Fig. 10. Time dependent measurement for comparing the drift estimation between fluorescent beads and our speckle-based method in a 3D SMLM experiment. For the speckle-based method, the laser with a wavelength of 488 nm was used to illuminate the sample; and the laser with a wavelength of 647 nm was used to excite the fluorescence beads. (a) Axial and (b) lateral drift measurements for x and y separately. The shaded areas are given by the averaged standard deviation of all bead localizations.

Biomedical Optics EXPRESS

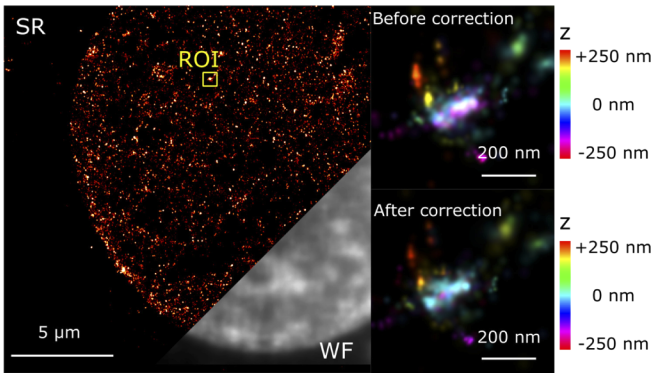

Fig. 11. The intensity sum projection of the drift corrected 3D SMLM image of a nucleus labeled with the DNA dye SytoxOrange [23], excited by the laser with a wavelength of 561 nm. Inset: color-coded maximum intensity projection before and after correction. The color scale indicates the z position.

5. Conclusion

We presented a three-dimensional drift estimation method for SMLM, based on speckle image correlation. We used low laser power to illuminate eukaryotic cell samples and image the backscattered laser light showing distinct speckle patterns. Because the structure of cells is unique, this method provides straightforward three-dimensional spatial information of the sample, which can be used for high-resolution drift estimation.

This method is expected to be especially useful in long term, high precision 3D SMLM measurements such as biological studies of nuclear genome architecture [24,25], because no fluorescent signals are required and the illumination power is kept low. Without additional sample preparation, sufficient blinking data points from SMLM measurements or advanced modification of the microscope setup, this method results in a highly precise drift estimation comparable with a fiducial markers approach. This method also provides an alternative drift correction approach for microscope systems equipped only with a single laser.

In this report, we demonstrated a speckle-based drift correction method for use in 3D SMLM in three dimensions. In the future, we plane to implement a second camera monitoring the speckle pattern during the SMLM image acquisition. The speckle-based method, especially when combined with a feedback mechanism, is expected to also find numerous applications in other imaging modes that need to keep the focus stable. If combined with a precise XY stage control, it can also serve to avoid lateral drifts during imaging. We expect that this method provides an alternative solution for highly precise drift correction in three dimensions in real time.

Funding

Boehringer Ingelheim Stiftung, Mainz/Germany; International PhD Programme on Gene Regulation, Epigenetics & Genome Stability, Mainz/Germany.

Acknowledgment

The authors thank the microscope core facility of the IMB for providing U2OS cells for the measurements, the electronic and the mechanic workshop for manufacturing electronic boards and mechanic elements. Dr. Sandra Ritz and Dr. Márton Gelléri helped proof reading of the manuscript. R.H. acknowledges funding by the Deutsche Forschungsgemeinschaft (DFG)

Biomedical Optics EXPRESS

via SFB TR166 "Receptorlight'", TP A4 and the Collaborative Research Center SFB 1278 (PolyTarget, project C04).

Disclosures

The authors declare that there are no conflicts of interest related to this article.

References

1. M. J. Rust, M. Bates, and X. Zhuang, "Sub-diffraction-limit imaging by stochastic optical reconstruction microscopy (STORM)," Nat. Methods **3**(10), 793–796 (2006).
2. E. Betzig, G. H. Patterson, R. Sougrat, O. W. Lindwasser, S. Olenych, J. S. Bonifacino, M. W. Davidson, J. Lippincott-Schwartz, and H. F. Hess, "Imaging Intracellular Fluorescent Proteins at Nanometer Resolution," Science **313**(5793), 1642–1645 (2006).
3. P. Lemmer, M. Gunkel, D. Baddeley, R. Kaufmann, A. Urich, Y. Weiland, J. Reymann, P. Müller, M. Hausmann, and C. Cremer, "SPDM: light microscopy with single-molecule resolution at the nanoscale," Appl. Phys. B: Lasers Opt. **93**(1), 1–12 (2008).
4. C. Cremer and B. R. Masters, "Resolution enhancement techniques in microscopy," Eur. Phys. J. H **38**(3), 281–344 (2013).
5. M. J. Mlodzianoski, J. M. Schreiner, S. P. Callahan, K. Smolková, A. Dlasková, J. Šantorová, P. Ježek, and J. Bewersdorf, "Sample drift correction in 3D fluorescence photoactivation localization microscopy," Opt. Express **19**(16), 15009–15019 (2011).
6. Y. Wang, J. Schnitzbauer, Z. Hu, X. Li, Y. Cheng, Z.-L. Huang, and B. Huang, "Localization events-based sample drift correction for localization microscopy with redundant cross-correlation algorithm," Opt. Express **22**(13), 15982–15991 (2014).
7. R. Han, L. Wang, F. Xu, Y. Zhang, M. Zhang, Z. Liu, F. Ren, and F. Zhang, "Drift correction for single-molecule imaging by molecular constraint field, a distance minimum metric," BMC Biophys. **8**(1), 1–14 (2015).
8. S. H. Lee, M. Baday, M. Tjioe, P. D. Simonson, R. Zhang, E. Cai, and P. R. Selvin, "Using fixed fiduciary markers for stage drift correction," Opt. Express **20**(11), 12177–12183 (2012).
9. H. Ma, J. Xu, J. Jin, Y. Huang, and Y. Liu, "A simple marker-assisted 3D nanometer drift correction method for superresolution microscopy," Biophys. J. **112**(10), 2196–2208 (2017).
10. A. Balinovic, D. Albrecht, and U. Endesfelder, "Spectrally red-shifted fluorescent fiducial markers for optimal drift correction in localization microscopy," J. Phys. D: Appl. Phys. **52**(20), 204002 (2019).
11. Y. Youn, Y. Ishitsuka, C. Jin, and P. R. Selvin, "Thermal nanoimprint lithography for drift correction in super-resolution fluorescence microscopy," Opt. Express **26**(2), 1670–1680 (2018).
12. S. A. Jones, S. H. Shim, J. He, and X. Zhuang, "Fast, three-dimensional super-resolution imaging of live cells," Nat. Methods **8**(6), 499–505 (2011).
13. M. Guizar-Sicairos, S. T. Thurman, and J. R. Fienup, "Efficient subpixel image registration algorithms," Opt. Lett. **33**(2), 156–158 (2008).
14. R. McGorty, D. Kamiyama, and B. Huang, "Active microscope stabilization in three dimensions using image correlation," Opt. Nanoscopy **2**(1), 3–7 (2013).
15. S.-Y. Chen, F. Bestvater, W. Schaufler, R. Heintzmann, and C. Cremer, "Patterned illumination single molecule localization microscopy (piSMLM): user defined blinking regions of interest," Opt. Express **26**(23), 30009–30020 (2018).
16. J. W. Goodmann, "Some fundamental properties of speckle*," J. Opt. Soc. Am. **66**(11), 1145–1150 (1976).
17. J. B. Pawley, *Handbook of Biological Confocal Microscopy* (Springer, 2006), Chap. 9.
18. M. Draijer, E. Hondebrink, T. van Leeuwen, and W. Steenbergen, "Review of laser speckle contrast techniques for visualizing tissue perfusion," Lasers Med. Sci. **24**(4), 639–651 (2009).
19. B. Huang, W. Wang, M. Bates, and X. Zhuang, "Three-dimensional super-resolution imaging by stochastic optical reconstruction microscopy," Science **319**(5864), 810–813 (2008).
20. H. P. Kao and A. S. Verkman, "Tracking of single fluorescent particles in three dimensions: use of cylindrical optics to encode particle position," Biophys. J. **67**(3), 1291–1300 (1994).
21. A. Szczurek, L. Klewes, J. Xing, A. Gourram, U. Birk, H. Knecht, J. W. Dobrucki, S. Mai, and C. Cremer, "Imaging chromatin nanostructure with binding-activated localization microscopy based on DNA structure fluctuations," Nucleic Acids Res. **45**(8), e56 (2017).
22. M. Ovesný, P. Křížek, J. Borkovec, Z. Švindrych, and G. M. Hagen, "ThunderSTORM: a comprehensive ImageJ plug-in for PALM and STORM data analysis and super-resolution imaging," Bioinformatics **30**(16), 2389–2390 (2014).
23. A. Szczurek, U. Birk, H. Knecht, J. Dobrucki, S. Mai, and C. Cremer, "Super-resolution binding activated localization microscopy through reversible change of DNA conformation," Nucleus **9**(1), 182–189 (2018).
24. T. Cremer, M. Cremer, B. Hübner, H. Strickfaden, D. Smeets, J. Popken, M. Sterr, Y. Markaki, K. Rippe, and C. Cremer, "The 4D nucleome: Evidence for a dynamic nuclear landscape based on co-aligned active and inactive nuclear compartments," FEBS Lett. **589**(20 PartA), 2931–2943 (2015).

Biomedical Optics EXPRESS

25. T. Cremer and C. Cremer, "Chromosome territories, nuclear architecture and gene regulation in mammalian cells," Nat. Rev. Genet. **2**(4), 292–301 (2001).